RSC Advances

PAPER

View Article Online
View Journal | View Issue

Cite this: *RSC Adv.*, 2014, **4**, 41212

Cellulose-derived carbon bearing –Cl and –SO_3H groups as a highly selective catalyst for the hydrolysis of cellulose to glucose†

Qi Pang, Liqing Wang, Hui Yang, Lishan Jia,* Xinwei Pan and Chenchao Qiu

Received 10th June 2014
Accepted 4th August 2014

DOI: 10.1039/c4ra05520a

www.rsc.org/advances

A solid acid catalyst (HA–CC–SO_3H) was synthesized by the sulfonation of amorphous carbon derived from the carbonization of dilute hydrochloric acid-pretreated microcrystalline cellulose. It was found that Cl^- ions are grafted onto the cellulose-derived carbon and affect the composition and structure of the carbon carrier during the carbonization process. The electrons of the aromatic carbons transfer to –Cl and –SO_3H groups, which influence their electronic state. In the cellulose hydrolysis process, the active electronic states make the –Cl groups more liable to form hydrogen bonds with cellulose, and the –SO_3H groups with stronger acidity easily break the glycosidic bonds of cellulose to produce glucose. The HA–CC–SO_3H catalyst exhibits excellent glucose selectivity (95.8%) at a moderate temperature (155 °C) under hydrothermal conditions.

Introduction

Cellulose is a major source of glucose, and its common hydrolysis methods include enzymatic hydrolysis and acidic hydrolysis.[1–4] Though enzymatic hydrolysis can obtain high selectivity, it requires long reaction times and rigorous conditions.[5] Liquid acid hydrolysis usually operates at high temperatures to obtain a high conversion rate, but it often has low glucose selectivity due to the formation of undesirable by-products.[1] Moreover, homogeneous catalysts also have other drawbacks such as equipment corrosion, difficult product separation, and catalyst recycling.[1,6]

In recent years, several kinds of solid acid catalysts have been used to hydrolyze cellulose, such as a Ru catalyst supported on heteropolyacids,[7] the H-form zeolite,[6,8] and acid-activated montmorillonite.[8,9] Among the various types of catalysts, sulfonated solid acids have superior catalytic activity[10–12] with the sulfonic group serving as the main active catalytic center.

Some researchers have introduced –Cl groups into solid acid catalysts to further improve catalytic performance. For example, Li and Pan synthesized a sulfonated chloromethyl polystyrene resin for hydrolyzing cellulose.[12] Hu *et al.* employed sucralose as a chlorine precursor for solid acid catalyst synthesis.[13] Shen *et al.* prepared a carbon-based solid acid upon sulfonation of cocarbonized starch and polyvinyl chloride.[14] These catalysts have all showed excellent catalytic activity in the hydrolysis of cellulose. The authors considered the –Cl groups act as cellulose-binding sites through hydrogen bonds formed by attacking the cellulose hydroxyl protons, and reduce the steric hindrance between the –SO_3H groups and glycosidic bonds.[14] However, existing catalysts are prepared using costly materials like sucralose and polyvinyl chloride. Because of the limited types of chemicals containing chlorine in carbohydrates and resin materials, the exploration of carbon-based solid acids containing –Cl groups is restricted. Moreover, these hydrolysis processes are often time consuming and usually require the pretreatment of cellulose. Thus, we have employed hydrochloric acid as a cheap and widely available source of chlorine to soak microcrystalline cellulose, which is carbonized later to load Cl^- ions onto the carbon carrier, in order to synthesize a highly selective catalyst for the one-step hydrolysis of cellulose.

In this paper, we synthesized a highly selective cellulose-derived carbon containing –Cl and –SO_3H groups, named the HA–CC–SO_3H catalyst, and used it to hydrolyze cellulose under hydrothermal conditions. In the preparation process, Cl^- ions adsorb onto cellulose to break the interchain hydrogen bonds in cellulose, and then graft onto its aromatic structure through carbonization. Moreover, –Cl groups influence the composition and structure of the cellulose-derived carbon, and make the HA–CC–SO_3H catalyst more stable. We show the effect of the preparation process and active groups (–Cl and –SO_3H groups) on the catalytic activity of the catalyst. Likewise, we propose the mechanism involved in the high glucose selectivity of the HA–CC–SO_3H-catalyzed reaction.

Department of Chemical and Biochemical Engineering, College of Chemistry and Chemical Engineering, Xiamen University, Xiamen 361005, Fujian, China. E-mail: jials@xmu.edu.cn; Fax: +86-592-2184822; Tel: +86-592-2188283

† Electronic supplementary information (ESI) available. See DOI: 10.1039/c4ra05520a

Results and discussion

Characterization of the HA–CC–SO_3H catalyst

The SEM images of microcrystalline cellulose and the sulfonated carbon carrier derived from the carbonization of hydrochloric acid-pretreated microcrystalline cellulose catalyst (HA–CC–SO_3H) are shown in Fig. 1(a and b). It is clear that the catalyst particles are cellulose-derived carbon fragments, which are smaller than microcrystalline cellulose in average size. It might be because hydrochloric acid absorbs on cellulose and facilitates hydrogen bonds cleavage during carbonization, which affects the morphology of the cellulose-derived carbon.

As illustrated in Fig. 2, the crystallographic diffraction peaks of microcrystalline cellulose at about $2\theta = 34°$ for the (040) plane, 14° for the (101) plane and 16° for the $(10\bar{1})$ plane disappear in the pattern for HA–CC–SO_3H.[8] Instead, the XRD pattern of HA–CC–SO_3H shows a weak and wide diffraction peak at around 24°, which is attributed to the (002) plane of the micrographites oriented in a random way, and a new weak diffraction peak at around 44°, which corresponds to the (100) axis of the graphite structure.[15] These diffraction peaks are related to amorphous carbon composed of aromatic carbon sheets oriented in a considerably random fashion.[16] This result suggests that the HA–CC–SO_3H catalyst is composed of amorphous carbon, aromatic rings, and even polycyclic structures.

The FT-IR pattern of HA–CC–SO_3H is depicted in Fig. 3. The absorption peaks at around 3428 cm^{-1} and 2923 cm^{-1} are attributed to the stretching vibrations of hydroxyl (–OH) groups[8] and C–H groups,[15] respectively. In addition, the band at about 1702 cm^{-1} is due to the bending vibration of C=O bonds.[14,15] These peaks are attributed to incomplete carbonization or oxidation of concentrated sulfuric acid, implying that this catalyst contains –OH and carboxyl (–COOH) groups.[14] A strong absorption peak at 1600 cm^{-1} caused by aromatic C=C stretching vibration,[17] also suggests the existence of aromatic ring structures. The peaks at around 1181 and 1039 cm^{-1} are assigned to O=S=O and –SO_3H stretching vibrations, respectively, suggesting –SO_3H groups are introduced into HA–CC–SO_3H.[13,14] Comparing HA–CC and HA–CC–SO_3H spectra with the CC spectrum, two absorption peaks appear at 832 and 880 cm^{-1}, which are assigned to C–H deformation aromatic bonds and out-of-plane O–H deformation bonds,[18] respectively.

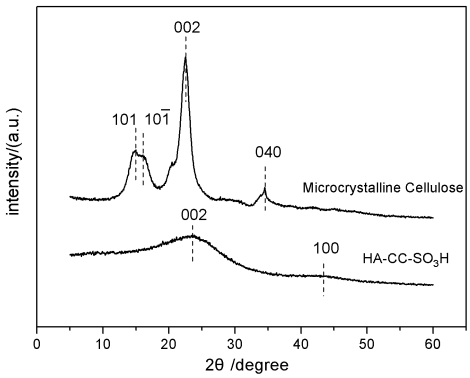

Fig. 2 The powder XRD patterns of HA–CC–SO_3H and microcrystalline cellulose.

It is supposed that Cl^- ions interact with cellulose during carbonizing, and finally affect the structure of the cellulose-derived carbon. However the absorption peaks, which are attributed to C–Cl bonds in the range of 500–700 cm^{-1} are weak.[19] To further investigate these functional groups, XPS measurements were carried out.

The XPS results for HA–CC–SO_3H are shown in Fig. 4. Fig. 4(a) gives the high-resolution Cl 2p spectrum of HA–CC–SO_3H. The strong peak obtained can be divided into two individual

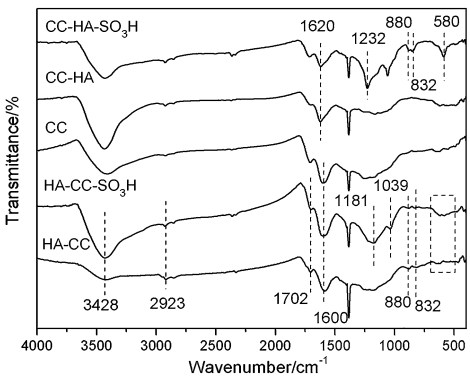

Fig. 3 The FT-IR spectra of the catalysts.

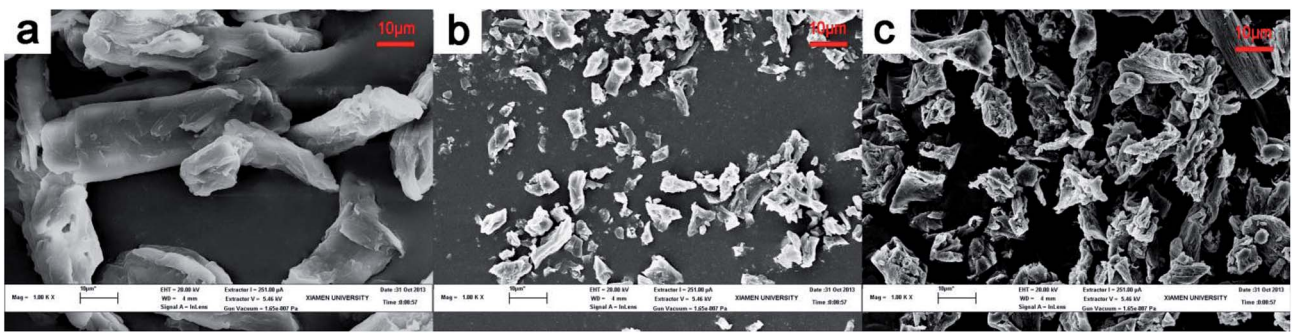

Fig. 1 SEM images of microcrystalline cellulose (a), HA–CC–SO_3H (b) and CC–HA–SO_3H (c). Observation conditions: extractor voltage is 5.46 kV, work distance is 4 mm and magnification is 1000.

peaks at about 199.5 eV and 201.1 eV, which are assigned to Cl 2p 3/2 and Cl 2p 1/2, respectively, suggesting that the –Cl groups are covalently bonded to the carbons in HA–CC–SO_3H including aromatic carbons.[14] The S 2p spectrum of HA–CC–SO_3H is shown in Fig. 4(b), the S 2p 3/2 and S 2p 1/2 peaks at 168.6 and 169.8 eV, respectively are assigned to –SO_3H groups, which indicates that –SO_3H groups are introduced into the catalyst upon sulfonation.[14,20]

The mechanism of high selectivity

As shown in Table 1, among a series of prepared analogous catalysts, HA–CC–SO_3H exhibits a relatively above average conversion, and its glucose selectivity can reach 95.8%. Through comparison, we tried to find out the reason for its high selectivity. Cellulose-derived carbon (CC) provides almost an equally poor performance as that found without catalyst, therefore CC has no catalytic ability. When loaded with –Cl and –SO_3H groups separately, hydrochloric acid-treated cellulose-derived carbon (CC–HA) and sulfonated cellulose-derived carbon (CC–SO_3H) can only increase conversion but not glucose selectivity. In addition, when prepared by a different –Cl group loading process, sulfonated hydrochloric acid-treated cellulose-derived carbon (CC–HA–SO_3H) obtains the highest conversion, but its glucose selectivity is only 52.9%. Thus, we are able to draw the conclusion that the existence of both –Cl and –SO_3H groups can be effective but not a sufficient condition for improving glucose selectivity.

Combining SEM micrographs (see Fig. 1(b and c)) and BET results (see Table S1 in the ESI†), HA–CC–SO_3H shows smaller particle size and a higher surface area than CC–HA–SO_3H, which suggests more active sites and better contact between the catalyst and reactant for HA–CC–SO_3H to facilitate the hydrolysis reaction. Moreover, its smaller average pore radius avoids product access and makes excessive hydrolysis of cellulose less likely. In addition, the TG results shown in Fig. 5 show clearly that the TG curves of the two catalysts both have two weight loss steps below 300 °C, which are attributed to the evaporation of imbibed water[8] and gasification of oxide, respectively. However, the TG curve of HA–CC–SO_3H shows relatively gentle slopes as the temperature increases, indicating that HA–CC–SO_3H is relatively stable and hard to break at high temperatures when compared to the CC–HA–SO_3H catalyst. Taking the preparation process into consideration, the differences of the two catalysts may be caused by the order of the dilute hydrochloric acid soaking and carbonization process. For HA–CC–SO_3H, hydrochloric acid absorbs on cellulose to break the interchain hydrogen bonds, making cellulose break into pieces and facilitates the production of aromatic carbon through carbonization; thus this catalyst is more stable.

Table 2 shows the compositions of the catalysts. Obviously, comparing with compositions of CC, the content of carbon increases greatly in the carbon carrier derived from the carbonization of hydrochloric acid-pretreated microcrystalline cellulose (HA–CC), which indicates Cl^- ions affect the elemental composition of cellulose-derived carbon during the carbonization process. However, the dilute hydrochloric acid soaking process makes –Cl groups form on this carbon carrier, leading to a significant decrease in the carbon content in CC–HA. Since the catalysts introduced –SO_3H groups by sulfonation, the content of oxygen increases resulting in a decreased carbon content in both HA–CC–SO_3H and CC–HA–SO_3H.[15]

Upon inspection of the FT-IR spectra in Fig. 3, HA–CC shows a characteristic peak for aromatic C=C stretching vibrations at about 1600 cm^{-1}, as well as CC, which clearly shows aromatic rings and polycyclic aromatic hydrocarbons are formed. The CC–HA and CC–HA–SO_3H spectra show a 20 cm^{-1} blue shift at about 1600 cm^{-1}, which is caused by electronic effects arising from the interaction between the –Cl groups and carbon carrier. In addition, the CC–HA–SO_3H spectrum shows two new strong peaks at 1232 cm^{-1} and 580 cm^{-1} after sulfonation, which are caused by C–O stretching vibrations[21] and characteristic double 6-membered ring vibrations,[22] respectively. These suggest the carbon carrier in CC–HA, which has a low stability is further oxidized during the sulfonation process to get its functional groups and structure change in CC–HA–SO_3H. Therefore, the low BET surface area may be caused by a collapse of the partial micropores in the carbon carrier during sulfonation.

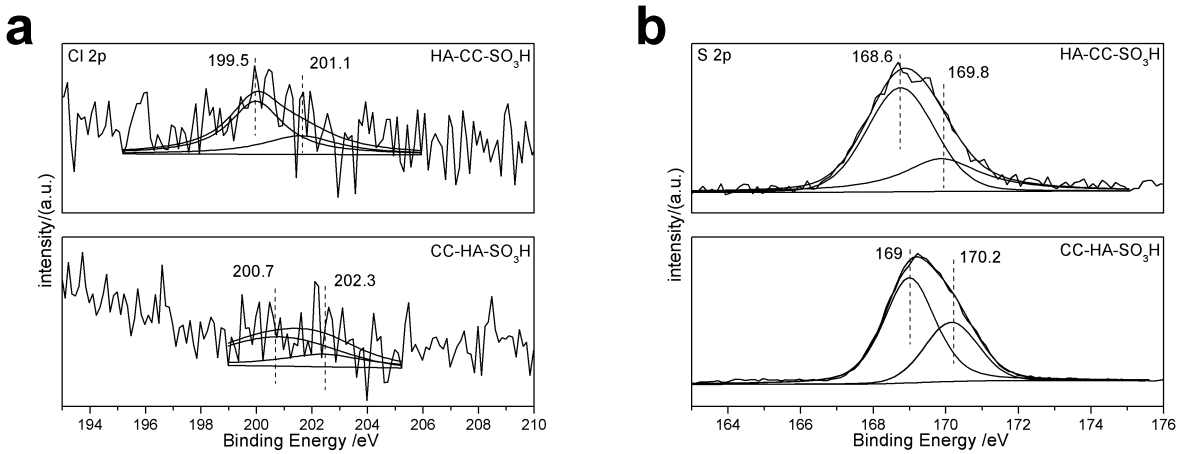

Fig. 4 The XPS spectra of HA–CC–SO_3H and CC–HA–SO_3H.

Table 1 The catalytic performance of the catalysts[a]

Sample	Time (h)	Temp (°C)	Conversion (%)	Selectivity (%)		
				Glucose	WSSs	WSOCs
None	4	155	4.8	47.9	13.3	38.8
CC	4	155	5.6	44.6	15.6	39.8
CC–HA	4	155	10.4	41.3	18.4	40.3
CC–SO_3H	4	155	9.9	48.5	25.1	26.4
HA–CC–SO_3H	4	155	11.3	95.8	1.9	2.3
CC–HA–SO_3H	4	155	17.4	52.9	24.7	22.4

[a] Reaction conditions: catalyst 50 mg, cellulose 200 mg, distilled water 40 mL.

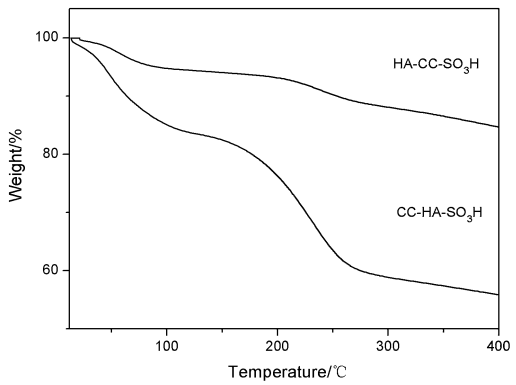

Fig. 5 Thermogravimetric curves of HA–CC–SO_3H and CC–HA–SO_3H.

Table 2 Elemental analysis results of catalysts

Sample	C%	H%	S%
CC	65.63	2.37	0
HA–CC	75.97	2.43	0
HA–CC–SO_3H	65.08	2.36	1.91
CC–HA	58.42	1.99	0
CC–HA–SO_3H	42.25	2.81	7.15

The XPS spectra were used to investigate the chemical combination state of HA–CC–SO_3H and CC–HA–SO_3H as shown in Fig. 4. The Cl 2p spectra for the HA–CC and CC–HA samples exhibit nearly no difference, which both show Cl 2p 3/2 and Cl 2p 1/2 peaks at 200.2 eV and 201.8 eV, respectively (see Fig. S1 in the ESI†). However, there is a 0.7 eV shift of the chlorine atom binding energy to a lower energy in the HA–CC–SO_3H spectrum when compared with the HA–CC spectrum. While in the Cl spectrum of CC–HA–SO_3H, a 0.5 eV shift towards a higher energy is observed, and the binding energy peak becomes very weak, which suggests the surface chlorine concentration reduces (see Table S2 in the ESI†). Moreover, the S 2p peaks in the HA–CC–SO_3H spectrum have a negative shift of 0.4 eV when compared with those in the CC–HA–SO_3H spectrum. These may be caused by the differences in the components and structure of the catalysts and electronic states changes of the functional groups.

For HA–CC, since a portion of –Cl groups graft within the aromatic structure and affect the structure of the carbon carrier, HA–CC is stable. Therefore during the sulfonation process, the –SO_3H groups are only loaded on the carbon carrier instead of replacing the –Cl groups, and the electrons in the aromatic structure flow to the –Cl and –SO_3H groups, resulting in a new charge balance. It is for these reasons that the Cl and S atoms have a relatively low binding energy in the HA–CC–SO_3H spectrum. For CC–HA–SO_3H, the Cl^- ions just form C–Cl bonds on the outer-plane of the carbon carrier; hence, –Cl groups are easily replaced by plenty of –SO_3H groups,[12] leading to the weak Cl 2p binding energy peak and increased sulphur content.

In the cellulose hydrolysis process, the –Cl group as electron donors attack the hydroxyl groups and hydrogen bonds on the intermolecular chains of cellulose, tending to form hydrogen bonds with cellulose.[13,14] The active electronic states and strong electronegativity of the –Cl groups in HA–CC–SO_3H, which has high hydrogen bond basicity to contribute to the formation of more hydrogen bonds. These hydrogen bonds can fix catalyst particles onto cellulose to increase the number of contact sites for –SO_3H groups to easily cleave the glycosidic bonds in cellulose. For –SO_3H, more received electrons results in stronger acidity, which accelerates glycosidic bond cleavage to obtain more glucose. Given all of this, HA–CC–SO_3H, which combines advantages of both –Cl and –SO_3H groups without doubt performs best for the hydrolysis of cellulose. The root causes of high glucose selectivity are the method used to prepare the cellulose-derived carbon bearing –Cl groups and the electronic states of the functional groups.

Durability experiments of catalyst

As shown in Fig. 5, the thermal stability of HA–CC–SO_3H was examined by thermogravimetric analysis, and the TG curve for the HA–CC–SO_3H catalyst shows good thermal stability. The durability of HA–CC–SO_3H was examined by recycling experiments over three cycles. Fig. 6 shows the conversion and glucose selectivity keep stable after recycling three times, indicating that the catalyst displays good stability in catalytic activity. Moreover, as shown in Fig. 7, in the FT-IR spectra of HA–CC–SO_3H, all the main characteristic peaks are still identified clearly. This

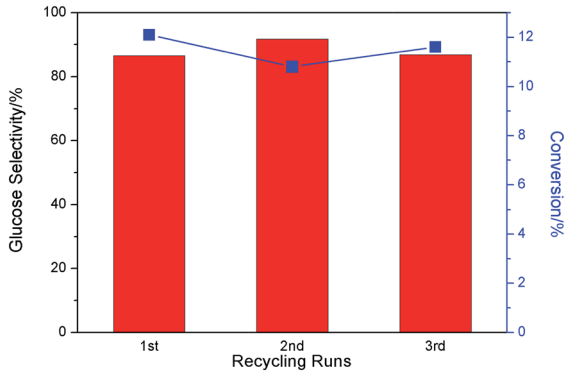

Fig. 6 Recycling experiments for HA–CC–SO_3H. Reaction conditions: catalyst 50 mg, cellulose 200 mg, distilled water 40 mL, 155 °C, 4 h. The catalyst and unreacted cellulose were recovered by filtration, washed, dried at 80 °C overnight, and directly used for the next reaction upon the addition of fresh cellulose.

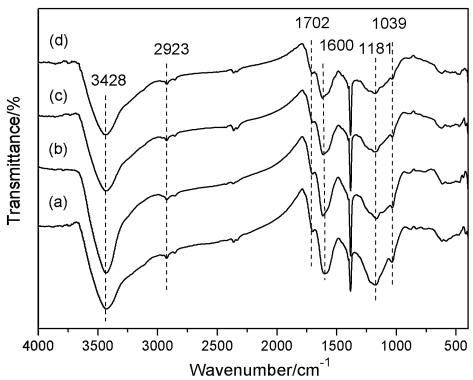

Fig. 7 FT-IR spectra of the HA–CC–SO_3H catalyst: fresh (a), 1st run (b), 2nd run (c), 3rd run (d).

illustrates the chemically bonded –Cl and –SO_3H groups on HA–CC–SO_3H do not have a leaching problem that happens to most carbon based-solid catalysts. Thus, the catalyst has excellent stability and good repeatability.

Conclusions

A cellulose-derived solid acid catalyst bearing –Cl and –SO_3H groups named HA–CC–SO_3H was synthesized. We employed the catalyst in the hydrolysis of cellulose and it exhibits strong potential for increasing glucose selectivity. Large amounts of –Cl formed on cellulose-derived carbon during the carbonization of diluted hydrochloric acid-impregnated microcrystalline cellulose, and they affected the content of aromatic carbon in the carbon carrier. This aromatic structure not only affects the electronic states of the –Cl and –SO_3H groups, but also enhances the stability of the catalyst. The active electronic states and strong electronegativity make the –Cl groups easily form hydrogen bonds with cellulose; thus, the –SO_3H groups with strong acidity have sufficient contact with cellulose to accelerate the cleavage of its glycosidic bonds for high glucose selectivity. In addition, the durability experiments and characterization indicate that the HA–CC–SO_3H catalyst has good catalytic stability, and the active groups have no leaching problem. We consider that this method of introducing –Cl groups onto a carbon carrier may pave a way for the exploration of novel solid acid catalysts.

Experimental

Materials

Microcrystalline cellulose was purchased from Alfa-Aesar. Hydrochloric acid (AR) and sulfuric acid (AR) were obtained from Sinopharm Chemical.

Synthesis of cellulose-derived carbon (CC) and sulfonated cellulose-derived carbon (CC–SO_3H). The cellulose-derived carbon (CC) was prepared using a high-temperature calcination method.[16] Microcrystalline cellulose was heated under a flow of N_2 for 1 h at 600 °C to produce a black solid, which was then ground to a black powder. CC was sulfonated by the addition of 98% sulfuric acid at 150 °C for 10 h. CC–SO_3H, was isolated by filtration, washed repeatedly, and dried at 80 °C overnight.

Synthesis of a sulfonated carbon carrier derived from the carbonization of hydrochloric acid-pretreated microcrystalline cellulose (HA–CC–SO_3H). The carbon carrier derived from the carbonization of hydrochloric acid-pretreated microcrystalline cellulose (HA–CC) was prepared according to a calcination method but with a slight modification. Microcrystalline cellulose was dipped in 10% HCl and stirred for 30 minutes before calcination. Using filtration, the HCl-pretreated microcrystalline cellulose was obtained. The conditions of calcination were according to synthesis of the cellulose-derived carbon (CC). The HA–CC was then sulfonated using 98% sulfuric acid at 150 °C for 10 h to produce the HA–CC–SO_3H catalyst.[23] The obtained catalyst was washed using deionized water until the liquid after washing is neutral. The catalyst was then washed with ethanol and dried in a drying oven at 80 °C overnight.

Synthesis of sulfonated hydrochloric acid-treated cellulose-derived carbon (CC–HA–SO_3H). The hydrochloric acid-treated cellulose-derived carbon (CC–HA) was prepared by impregnation method. The oven-dried CC and 10% HCl were added into a beaker and stirred at 80 °C for 10 hours in an oil bath. After cooling, the suspension was filtered and washed repeatedly with distilled water, and dried at 80 °C overnight. The CC–HA–SO_3H catalyst was obtained by sulfonating CC–HA, then filtered and washed by deionized water and ethanol, dried at 80 °C overnight.

Reactor and experiment conditions

The hydrolysis of cellulose was carried out in a thermal water kettle. Microcrystalline cellulose (200 mg), catalyst (50 mg), and water (40 mL) were introduced into the reactor, and heated at 155 °C for 4 h. The reaction mixture was separated by filtration after cooling. The filter residue was dried in drying oven at 80 °C.

The conversion of cellulose was calculated by the weight difference of dried cellulose before and after the reaction:

Conversion (%) =
(1 − weight of unreacted cellulose/weight of cellulose) × 100

The yield of glucose was calculated as follows:

Glucose yield (%) =
(weight of glucose × 0.9/weight of cellulose) × 100

where, 0.9 = molecular weight of $C_6H_{10}O_5$/molecular weight of $C_6H_{12}O_6$, and $C_6H_{10}O_5$: cellulose; $C_6H_{12}O_6$: glucose.[24]

The selectivities were calculated as follows:

Glucose selectivity (%) =
(yield of glucose/conversion of cellulose) × 100

WSSs selectivity (%) =
(yield of WSSs/conversion of cellulose) × 100

WSOCs selectivity (%) =
100 − glucose selectivity − WSSs selectivity

WSSs and WSOCs are denoted as water-soluble sugars except glucose and water-soluble organic compounds (*e.g.*, formic acid, acetic acid, furfural, hydroxymethyl furfural), respectively.

Product analysis

The concentration of water-soluble sugars was analyzed using High Performance Liquid Chromatography (HPLC). The analysis was performed using an Agilent series 1100 HPLC system equipped with a refractive index detector (RID) and a Hypersil ODS column at 30 °C for qualitative and quantitative measurement.

Water-soluble organic compounds were determined using a GCMS QP2010 Plus gas chromatography-mass spectrometer (GC-MS). The GC was equipped with a flame ionization detector and an Rtx-5MS capillary column.

Characterization

A PANalytical X'pert PRO X-ray diffractometer was used to record the X-ray diffraction pattern at room temperature from 5° to 60° with a scan rate of 20° min^{-1}, employing Cu Kα radiation (λ = 1.54056 Å). Scanning electron microscopy (SEM) analysis was conducted using a LEO 1530 scanning electron microscope. FT-IR spectra were recorded between 4000 and 400 cm^{-1} using a Nicolet Avatar 330 Fourier transform spectrometer with a standard KBr disk method. X-ray photoelectron spectroscopy (XPS) analysis was performed on a PHI Quantum 2000 Scanning ESCA microprobe with a monochromatized 75 microfocused Al X-ray source. The binding energy was calibrated by C 1s as reference energy (C 1s 284.8 eV). Elemental analysis was measured using a Elementar Vario EL III elemental analyzer (Elementar Analysen System GmbH, Germany). Thermogravimetric analysis (TG) was conducted using a SDT-Q600 thermogravimetric analyzer from room temperature to 800 °C under a flow of N_2. The Brunauer–Emmett–Teller (BET) surface area was measured by high-purity nitrogen gas adsorption using a Trister3000 adsorption instrument. The total pore volume and average pore radius were estimated from the N_2 desorption curves using BJH analysis.

Acknowledgements

This research is supported by the general program of the National Natural Science Foundation of China (Grant no. 21176203). The authors are grateful to the Analysis and Testing Centre of Xiamen University for the analysis and observation work in this study.

Notes and references

1 R. Rinaldi and F. Schuth, *ChemSusChem*, 2009, **2**, 1096–1107.
2 H. Peng, H. Li, H. Luo and J. Xu, *Bioresour. Technol.*, 2013, **130**, 81–87.
3 F. Guo, Z. Fang, C. C. Xu and R. L. Smith, *Prog. Energy Combust. Sci.*, 2012, **38**, 672–690.
4 M. G. Resch, B. S. Donohoe, J. O. Baker, S. R. Decker, E. A. Bayer, G. T. Beckham and M. E. Himmel, *Energy Environ. Sci.*, 2013, **6**, 1858–1867.
5 S. Tsubaki and J. Azuma, *Bioresour. Technol.*, 2013, **131**, 485–491.
6 Y.-B. Huang and Y. Fu, *Green Chem.*, 2013, **15**, 1095.
7 R. Palkovits, K. Tajvidi, A. M. Ruppert and J. Procelewska, *Chem. Commun.*, 2011, **47**, 576–578.
8 D. S. Tong, X. Xia, X. P. Luo, L. M. Wu, C. X. Lin, W. H. Yu, C. H. Zhou and Z. K. Zhong, *Appl. Clay Sci.*, 2013, **74**, 147–153.
9 K.-i. Shimizu and A. Satsuma, *Energy Environ. Sci.*, 2011, **4**, 3140.
10 C. Zhang, Z. Fu, Y. C. Liu, B. Dai, Y. Zou, X. Gong, Y. Wang, X. Deng, H. Wu, Q. Xu, K. R. Steven and D. Yin, *Green Chem.*, 2012, **14**, 1928.
11 D. Verma, R. Tiwari and A. K. Sinha, *RSC Adv.*, 2013, **3**, 13265.
12 L. Shuai and X. Pan, *Energy Environ. Sci.*, 2012, **5**, 6889.
13 S. Hu, T. J. Smith, W. Lou and M. Zong, *J. Agric. Food Chem.*, 2014, **62**, 1905–1911.
14 S. Shen, B. Cai, C. Wang, H. Li, G. Dai and H. Qin, *Appl. Catal., A*, 2014, **473**, 70–74.
15 Y. Jiang, X. Li, Q. Cao and X. Mu, *J. Nanopart. Res.*, 2010, **13**, 463–469.
16 S. Suganuma, K. Nakajima, M. Kitano, D. Yamaguchi, H. Kato and S. Hayashi, *J. Am. Chem. Soc.*, 2008, **130**, 12787–12793.
17 X. Xie, B. Goodell, D. Zhang, D. C. Nagle, Y. Qian, M. L. Peterson and J. Jellison, *Bioresour. Technol.*, 2009, **100**, 1797–1802.
18 R. Carter, C. Gierczak and R. Dickie, *Appl. Spectrosc.*, 1986, **40**, 649–655.
19 M. Wu, P. Painter and M. Coleman, *J. Polym. Sci., Polym. Phys. Ed.*, 1980, **18**, 95–110.
20 S. Suganuma, K. Nakajima, M. Kitano, D. Yamaguchi, H. Kato, S. Hayashi and M. Hara, *Solid State Sci.*, 2010, **12**, 1029–1034.

21 E. Soda, F. Koba, S. Kondo, S. Ogawa and S. Saito, *Proc. SPIE*, 2007, **6519**, 65192P.
22 C.-L. Zhang, S. Li, Y. Yuan, W.-X. Zhang, T.-H. Wu and L.-W. LIn, *Catal. Lett.*, 1998, **56**, 207–213.
23 Q. Zhang, M. Benoit, K. De Oliveira Vigier, J. Barrault, G. Jégou, M. Philippe and F. Jérôme, *Green Chem.*, 2013, **15**, 963.
24 W.-H. Chen, S.-C. Ye and H.-K. Sheen, *Appl. Energy*, 2012, **93**, 237–244.